Electronic Supplementary Material (ESI) for RSC Advances.

Supporting Information

Prussian blue nanoparticles for laser-induced photothermal therapy of tumors

Hilary A. Hoffman[a], Lina Chakrabarti[a,b], Matthieu F. Dumont[a], Anthony D. Sandler[a,b,c,d], and Rohan Fernandes[*a,d,e]

[a]The Sheikh Zayed Institute for Pediatric Surgical Innovation, Children's National Medical Center, 111 Michigan Ave NW, Washington, DC 20010

[b]The Joseph E. Robert Center for Surgical Care, Children's National Medical Center, 111 Michigan Ave NW, Washington DC 20010

[c]Department of Surgery, George Washington University, 2330 Eye St NW, Washington, DC 20037

[d]Department of Pediatrics, George Washington University, 2330 Eye St NW, Washington, DC 20037

[e]Department of Radiology, George Washington University, 2330 Eye St NW, Washington, DC 20037

This supporting information document contains: (1) Size and morphology of PB NPs; (2) Characterization of PB NPs; (3) Calculation of the photothermal conversion efficiency of PB NPs; (4) Statistical analysis; (5) Supporting information references

1. Size and morphology of PB NPs

We measured the particle size distribution of the PB NPs using dynamic light scattering (DLS; Figure S1A) and the size and morphology of the PB NPs using transmission electron microscopy (TEM; Figure S1B).

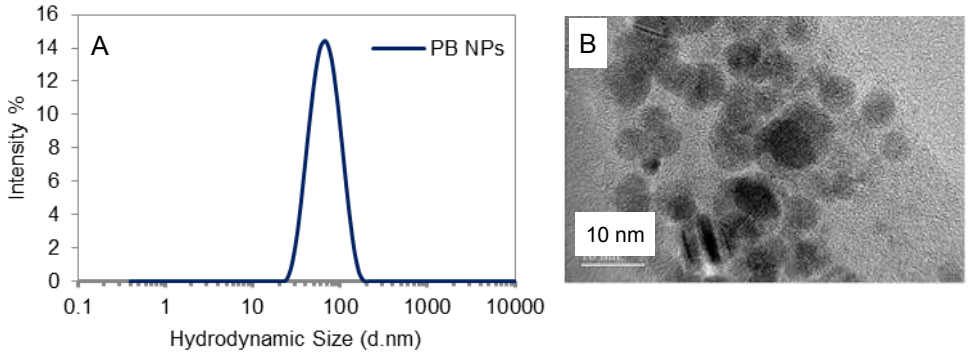

Figure S1. Size and morphology of PB NPs. (A) DLS of PB NPs showing the mean diameter (hydrodynamic size) of the PB NPs to be ~65 nm. (B) Representative TEM of PB NPs showing individual nanoparticles (Scale bar = 10 nm).

2. Characterization of PB NPs.

We characterized the PB NPs using Fourier transform infrared (FTIR; Figure S2A) spectroscopy and powder X-ray diffractometry (XRD; Figure S2B).

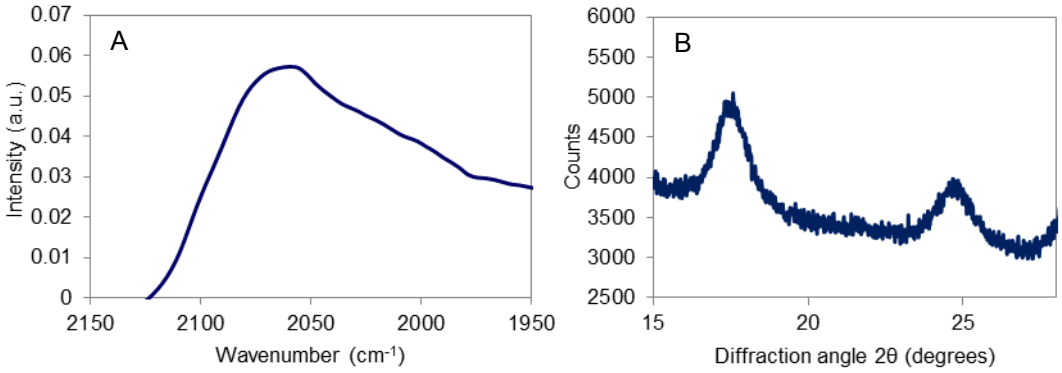

Figure S2. Characterization of PB NPs. (A) FTIR spectrum of PB NPs in the cyanide stretching region (1950 cm^{-1}-2300 cm^{-1}). (B) Room temperature XRD of PB NPs.

a. FTIR of PB NPs.

FTIR spectra of PB NPs were recorded on a Thermo Nicolet NEXUS 670 FTIR spectrometer fitted with a Smart Endurance 0033-897 ATR accessory. Typically, 16 scans were taken between 1940 cm^{-1} and 2100 cm^{-1} with a precision of 0.4 cm^{-1}. Powders of PB NPs were pressed against

a zinc selenide (ZnSe) ATR anvil. The FTIR spectrum of PB NPs exhibited a broad band at 2070 cm^{-1} corresponding to the Fe^{II}-CN-Fe^{III} cyanide stretch energy (Figure S2A).

b. Powder XRD of PB NPs.

XRD patterns of PB NPs were measured on a D8 Advance powder diffractometer using CuKα radiation from a sealed tube with a Ni β-filter equipped with Soller slits and a LynxEye position sensitive detector. PB NPs nanoparticles were carefully packed (without excessive pressure) in a zero-background sample holder and measured from 15 to 27° 2θ with 0.013° step sizes and a 0.6 s/step exposition. Peak fitting was performed on the Topas software (Bruker AXS) using a fundamental parameters approach. XRD of PB NPs exhibited two peaks corresponding to the 200 and 220 diffraction planes at 17.51 and 24.68 degrees (Figure S2B). These diffraction peaks were indexed to the Prussian blue lattice using the space group Fm-3m (No. 225) and confirmed the presence of one phase constituted by Prussian blue. Using the (220) reflections fitted to a Gaussian function, the lattice parameters were calculated. We found the following lattice constant for Prussian blue, a = 10.17 Å.

3. Calculation of photothermal conversion efficiency of PB NPs.

The photothermal conversion efficiency of PB NPs was calculated using the model described in Roper's *et al.*[1] where the photothermal conversion efficiency η_T is described by the following equation (refer to the main text for definitions of the individual terms of the following equation):

$$\eta_T = \frac{hA(T_{max} - T_{amb}) - Q_0}{I(1 - 10^{-A_\lambda})} \qquad (1)$$

The study was performed in a 96 well plate containing 200 µL of 1 mg/mL PB NPs. The sample was irradiated by an 808 nm near infrared (NIR) laser (1 W; 2.5 W/cm^2) and the system temperature was temporally measured until it reached its maximum temperature. At this point, the laser was turned off and the system temperature was temporally measured until it cooled to the ambient temperature. A similar study was performed using 200 µL water (Milli-Q water) and the heating-cooling curves were generated (Figure S2). The temperatures were measured using a Mini-Hypodermic Thermocouple Probe Model HYP-0 (Omega™). The well plate was aligned so that the laser beam covered the entire surface of the well to ensure uniform heating of the sample.

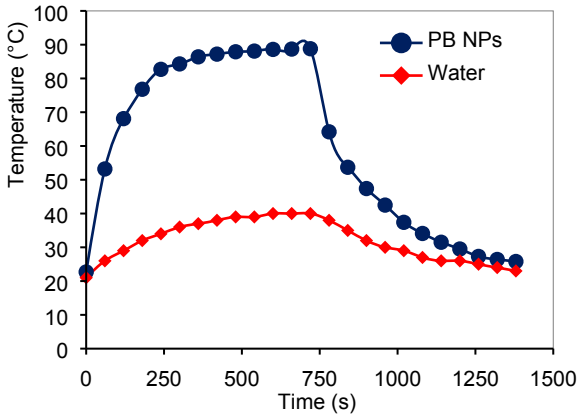

Figure S3. Heating and cooling curves of 1 mg/mL PB NPs and water (Milli-Q water) irradiated by an 808 nm NIR laser (1 W; 2.5 W/cm2). PB NPs attained a maximum temperature that was 48.8 ^{0}C > than that attained for water.

Plotting ln(ΔT) as a function of time for the cooling curves (after switching off the laser) for 1 mg/mL PB NPs and water at a laser power of 1 W or 2.5 W/cm^2 yielded a linear plot with the slope of the linear plot equaling $-1/\tau_s$ from which τ_s, the experimental system time constant was calculated. m_iC_i are the mass multiplied by the heat capacity for the sample. For our studies, m_i is 0.2 g and C_i is 4.187 J (g x K)$^{-1}$.

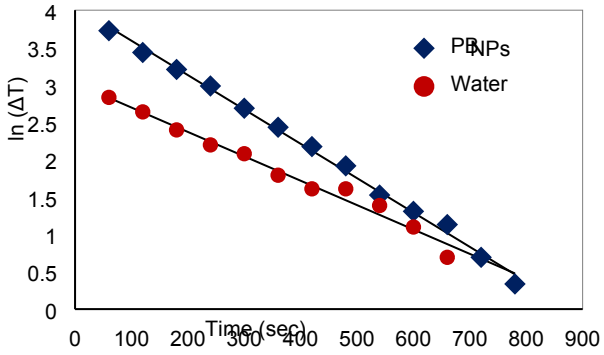

Figure S4. The cooling curves for 1 mg/mL PB NPs and water were linearly fit. The slopes of the linear fits, $-1/\tau_s$, were used to calculate τ_s for PB NPs and water. PB NPs had lower τ_s than water.

Using Equation 2, we calculated hA values of 0.00385 J s^{-1} K^{-1} for PB NPs and 0.00259 J s^{-1} K^{-1} for water.

$$\tau_s = \frac{m_i C_i}{hA} \qquad (2)$$

Where h is the heat transfer coefficient, and A is the heat transfer surface area of the system.

Using the measured values, we calculated Q_0 for water or rate of heat input due to absorption of light energy by water using Equation 3.

$$Q_0 = hA(T_{water\ max} - T_{water\ amb}) \qquad (3)$$

Equation 3 yielded a Q_0 value of 0.04929 J s^{-1} which was used to calculate η_T according to Equation 1 where I($1 - 10^{-A_\lambda}$) equaled 1. By this method we calculated a photothermal conversion efficiency of 20.5% for our PB NPs.

3. Statistical analysis

A 3-way ANOVA model was used to perform statistical analysis for the XTT assay (Figure 3) and animal (normalized tumor volume) studies (Figure 5B) by using the restricted maximum likelihood method as described by Thompson.[2]

Using the Thompson method to analyze the XTT assay results, we found a significant difference (decrease) in neuro2a viability at concentrations of 1.33 x 10^{-6} mg PB/cell (0.1 mg/mL) and 6.67 x 10^{-6} mg PB/cell (0.5 mg/mL) at the 48 hour time point as indicated by $p < 0.001$. As discussed in the main text, the conditions for the *in vivo* study were well below this cytotoxic range as we inoculated 1 million cells and injected the mice with 50 μL of 1 mg/mL of PB NPs into ~50 mm^3 volume tumors.

Using the Thompson method to analyze the normalized tumor volumes as a function of days post-treatment, we found a significant difference (decrease) in normalized tumors volume from Day 7 onward for the mice injected with PB NPs and irradiated with the NIR laser compared to the laser (no particles) and control (no treatment) groups.

4. Supporting information references.

1. K.D. Roper, W. Ahn, and M. Hoepfner, *J. Phys. Chem. C*, 2007, **111**, 3636-3641.

2. W.A. Thompson Jr, *Ann. Math. Statist.*, 1962, **33**, 273-289.